PROCEEDINGS OF SPIE

SPIEDigitalLibrary.org/conference-proceedings-of-spie

Q-band receiver system design for the Canadian DVA-2 radio telescope

Salem Hesari, S., Henke, D., Reshetov, V., Jiang, F., Seyfollahi, A., et al.

S. Salem Hesari, D. Henke, V. Reshetov, F. Jiang, A. Seyfollahi, L. B. G. Knee, L. Baker, J. Bornemann, D. Chalmers, "Q-band receiver system design for the Canadian DVA-2 radio telescope," Proc. SPIE 11453, Millimeter, Submillimeter, and Far-Infrared Detectors and Instrumentation for Astronomy X, 114533A (13 December 2020); doi: 10.1117/12.2562751

SPIE.

Event: SPIE Astronomical Telescopes + Instrumentation, 2020, Online Only

Downloaded From: https://www.spiedigitallibrary.org/conference-proceedings-of-spie on 14 Dec 2020 Terms of Use: https://www.spiedigitallibrary.org/terms-of-use

Q-band receiver system design for the Canadian DVA-2 radio telescope

S. Salem Hesari*[a], D. Henke[a], V. Reshetov[a], F. Jiang[a], A. Seyfollahi[a], L.B.G. Knee[a]
L. Baker[b], J. Bornemann[c], D. Chalmers[d]
[a] NRC Herzberg Astronomy and Astrophysics Research Centre, Victoria, BC, Canada
[b] EM Consultant, Issaquah, WA, United States of America
[c] University of Victoria, Victoria, BC, Canada
[d] NRC Dominion Radio Astrophysical Observatory, Kaleden, BC, Canada

ABSTRACT

A compact front-end system is presented for a dual-linear polarization cryogenic Q-band receiver. This receiver will be used to demonstrate the high frequency performance of the Dish Verification Antenna 2 (DVA-2) composite reflector telescope between 35–50 GHz and is a technology demonstrator with possible application to the National Radio Astronomy Observatory's Next Generation Very Large Array (ngVLA). A vacuum vessel and a two-stage Gifford-McMahon cryopump system are used for the cryogenic environment. The second stage of the cryostat is cooled to 16 K and includes a small choke ring feed horn, a low-loss noise calibration module (NCM) integrated with orthogonal mode transducer (OMT), and two cryogenically cooled mHEMT MMIC low-noise amplifiers (LNAs). Using a noise diode as the noise source on the 300 K stage inside the cryostat helps to protect the cooled components from signals outside of the cryostat, and also lessen the heat on the second stage since a noise diode normally produce a power dissipation of several hundred mW. The OMT design is an optimized version of the design used in the ALMA Band 1 cartridge with two integrated directional couplers and excellent performance. The cascaded noise analysis of the receiver shows a receiver noise temperature of 19.4 K.

Keywords: cryogenic, feed horn, OMT, LNA, Q-band, receiver, DVA2, ngVLA, linear, ALMA

1. INTRODUCTION

A cryogenic single pixel Q-band radio receiver covering the frequency range of 35 to 50 GHz is under development at the Millimeter Instrumentation Group (MIG) at NRC Herzberg in Victoria, Canada [1]. The purposes of designing this dual polarized receiver are to verify RF and optical performance of DVA-2 at the highest operating frequency, contribute to evaluation of composite-material antennas for millimeter-wave telescopes such as the next generation VLA (ngVLA), extend Herzberg Astronomy and Astrophysics Research Centre (HAA) low noise amplifier technology to Q-band frequency range, and provide a potential science receiver for DVA-2.

High demands toward the development of high frequency radio telescopes encourage the researcher to upgrade and improve Dish Verification Antenna DVA-1 at L-band and develop DVA-2 composite material dish to work up to Q-Band frequency range [2]. DVA-2 is a dual reflector, offset Gregorian configuration which provides a clear aperture with no blockage. The DVA-2 composite antenna has a primary surface accuracy goal of 0.335 mm RMS (unweighted) and 0.22 mm (weighted). Based on the Ruze Equation, the efficiency at 50 GHz is 81% for weighted surface error and 61% for unweighted surface error. For 30 GHz, weighted surface error gets us 93% and 84% for unweighted surface error in order to extend the useable frequency range up to 50 GHz which is an important stepping stone in the development of ngVLA-compliant antenna design. DVA-2 composite dish is a shaped optic with a wide half angle opening that is designed to map a -16 dB edge taper on the secondary. The shaped optic improves the aperture efficiency, and provide lower sidelobe and better wide angle spillover [3]. The specifications are presented in Table 1.

The Q-band receiver is an excellent platform to demonstrate various HAA-developed technologies, including cryogenic low noise amplifiers, a dual-linear orthomode transducer (OMT), LNA bias control and monitor and control boards, a wide-angle DVA2-compatible feed horn, a low loss vacuum window, and an injected noise calibration.

The component development of the cryogenic single pixel Q-band receiver including system analysis of front-end and back-end system are presented in the following sections.

Millimeter, Submillimeter, and Far-Infrared Detectors and Instrumentation for Astronomy X,
edited by Jonas Zmuidzinas, Jian-Rong Gao, Proc. of SPIE Vol. 11453, 114533A
© 2020 SPIE · CCC code: 0277-786X/20/$21 · doi: 10.1117/12.2562751

Downloaded From: https://www.spiedigitallibrary.org/conference-proceedings-of-spie on 14 Dec 2020
Terms of Use: https://www.spiedigitallibrary.org/terms-of-use

Table 1 DVA-2 specification

Edge taper on the primary reflector	-12 dB
Edge taper on the secondary reflector	-16 dB
Half opening angle	55-degree
Ruze efficiency at 30 GHz	93%
Ruze efficiency at 50 GHz	81%
Primary	15 m
Optics	Offset Gregorian
Illumination	Opening half-angle 55°

2. OVERALL SYSTEM DESCRIPTION

The cryogenically cooled single pixel Q-band receiver main specifications are presented in Table 2. A vacuum vessel and two-stage Gifford-McMahon cryopump system are used for cryogenic environment, which provides a 16 K and a 70 K stage. The front-end components including feed horn, OMT with two integrated 35 dB directional couplers for noise injection, and two LNAs with waveguide WR-22 input and output ports are located in 16 K stage. The vacuum window provides a smooth transition from the room temperature to the cooled stage. An mHEMT MMIC LNA with noise temperature about 12 K is under development. The proposed Q-band receiver provides a noise temperature lower than 20 K. The front-end and back-end block diagram of the proposed received is depicted in Figure 1 and Figure 2, respectively.

Table 2 Q-band Receiver Specifications

RF frequency range	35 – 50 GHz
Polarization	Dual-linear
Receiver noise temperature	T_{RX} < 20 K
Optics	Optimized for DVA-2 telescope
LNA noise temperature	T_{LNA} < 12 K
Calibration	Noise injection
Monitoring	Remote monitor and control
Cryogenic environment	2-stage Gifford-McMahon cryopump system (16 K and 70 K stages)

Downloaded From: https://www.spiedigitallibrary.org/conference-proceedings-of-spie on 14 Dec 2020
Terms of Use: https://www.spiedigitallibrary.org/terms-of-use

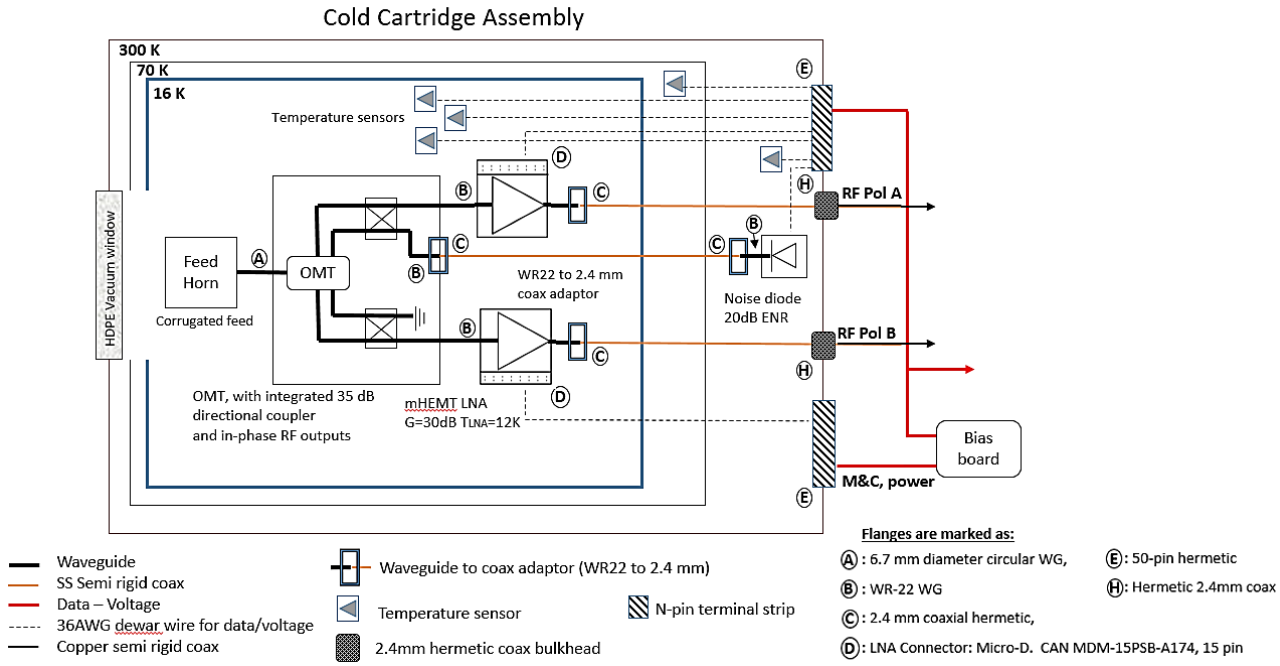

Figure 1 Front-end Q-band Receiver Electrical Block Diagram

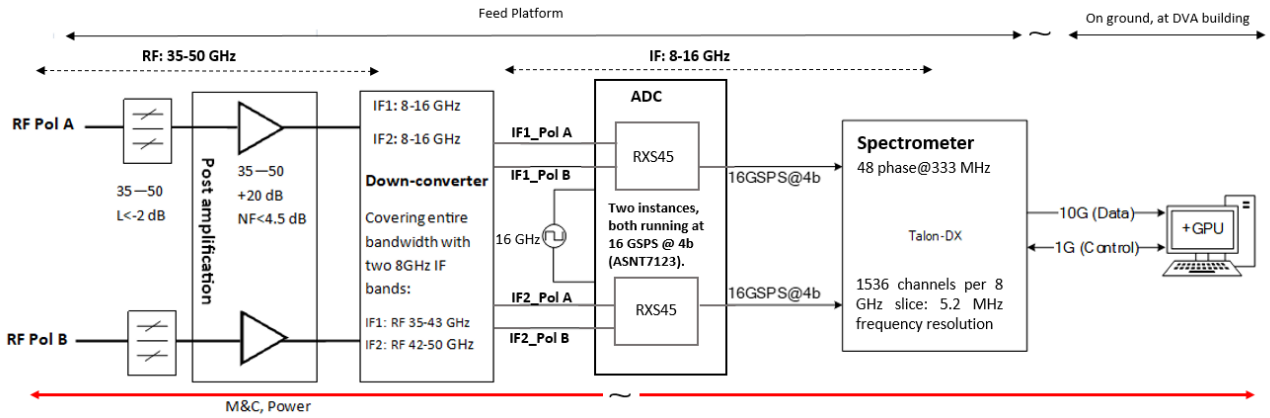

Figure 2 Back-end Q-band Receiver Electrical Block Diagram – Signal Conditioning, Downconverter, and Spectrometer

3. FEED HORN

The Q-band receiver feed horn has to match the DVA-2 optics. The requirement for this feed horn is a wide 55-degree half opening angle, 16 dB edge taper, input match greater than 20 dB, aperture efficiency better than 78%, symmetric radiation pattern, and sidelobe levels better than 20 dB. There are different kinds of feed horns available like quad ridged, conical, elliptical, and corrugated feed horns. Among all of them, a corrugated feed horn is chosen for the Q-band receivers since it meets all the requirements consisting symmetric E-plane, H-plane, and D-plane patterns, nearly constant beamwidth over the operating frequency range, low cross polarization, and great input match.

Figure 3 presents the axial corrugated feed horn and its measured and simulated reflection coefficient. The proposed feed horn was manufactured at NRC Herzberg in Victoria out of aluminum 6063. The input match S11 is better than -22 dB at the low end and better than -30 dB at the upper band. The feed horn will be installed inside the second stage of the cryostat to reduce the noise and removes the requirement to use a thermal transition between the feed and the cryogenic LNA.

Downloaded From: https://www.spiedigitallibrary.org/conference-proceedings-of-spie on 14 Dec 2020
Terms of Use: https://www.spiedigitallibrary.org/terms-of-use

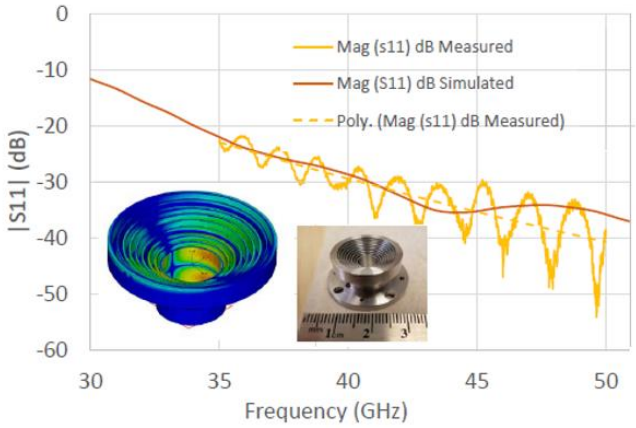

Figure 3 Corrugated feed horn, measured and simulated input match

An NSI planar nearfield scanner was used for the feed horn measurement. This near-field scanner has limited range and provides a scanning area of 400 mm x 400 mm which only covers angular beamwidth within $\theta = \pm 60°$ from boresight. As it is shown in [1], the proposed feed has excellent rotational symmetry. The radiation pattern of the proposed feed horn will be measured in a far-field anechoic chamber to cover the full rotational symmetry and the entire beamwidth in the future.

Table 3 shows the cross polarization level and side lobe level of the abovementioned feed horn across the frequency range. The cross polarization is measured at 45-degree plane since it has the worst cross polarization compare to $\varphi = 0°, 90°$. Figure 4 presents the efficiency calculation of the feed horn including amplitude efficiency, polarization efficiency, phase efficiency, spillover efficiency, and finally the aperture efficiency in 12 frequencies over the bandwidth. This calculation has been done by implementing a Post-Processing Template compatible with CST's optimizer and parameter sweep functions using VBA Macros, performing numerical integration over an antenna farfield result to calculate its aperture efficiency.

Table 3 Cross polarization and max sidelobe levels of the corrugated feed horn (simulated results)

Frequency (GHz)	**34**	**38**	**42**	**46**	**50**
Cross Polarization	-32.5 dB	-27.9 dB	-30 dB	-28.8 dB	-26.6 dB
Side Lobe Level	-33 dB	-27.7 dB	-30.6 dB	-32.3 dB	-26.7 dB

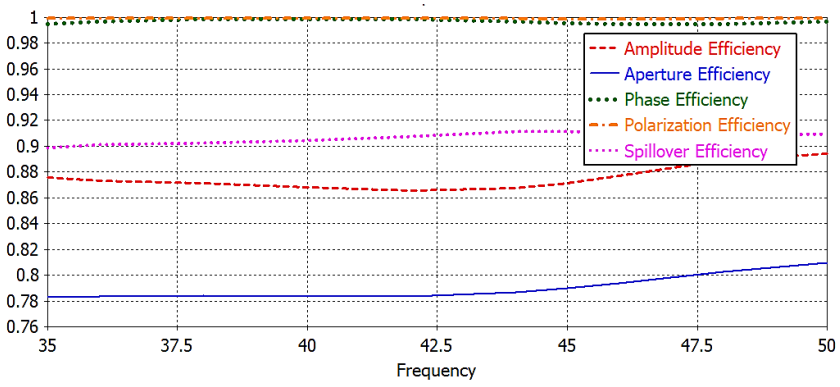

Figure 4 Efficiency calculations for the corrugated feed horn (CST simulated results)

4. VACUUM WINDOW

There are several factors a designer must take into account when design a vacuum window for an optical system, since vacuum window is the first optical component of the cartridge and can have an important role in the noise contribution.

Downloaded From: https://www.spiedigitallibrary.org/conference-proceedings-of-spie on 14 Dec 2020
Terms of Use: https://www.spiedigitallibrary.org/terms-of-use

Therefore, by minimizing the reflection coefficient, insertion loss, the dielectric loss, and also considering strength, bandwidth, environmental stability, and available coatings we can minimize the noise contribution of the vacuum window. HDPE (High-density polyethylene) with $\varepsilon_r = 2.33$, and $\tan\delta = 2.5e-04$ is chosen as the vacuum window material in order to maximize the aperture efficiency and minimize the noise temperature.

In order to improve the reflection properties of the vacuum window, we investigated the impact of various geometrical shapes and also multiple antireflection layers on the reflectivity and found out that the two antireflection layers with circular holes meet all the requirements. The specifications of the antireflection layer are stated in Table 4 and shown in Figure 5.

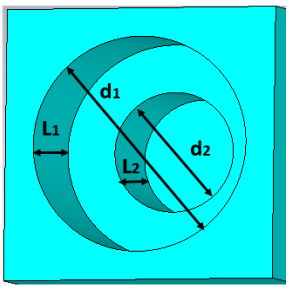

Figure 5 Parameters of the two layers antireflection layer

Table 4 Specifications of the two layer antireflection layer

Parameter	L_1	L_2	d_1	d_2	Pitch	εr_{HDPE}	$Tan\delta_{HDPE}$
Value	1.54 mm	1.33 mm	2.85 mm	1.5 mm	3.2 mm	2.33	2.5e-04

In addition, an investigation on the effect of different grid types on the reflectivity is done. A comparison between an HDPE window with two AR layers in XY grid and Hexagonal grid is done which is presented in Figure 6. The hexagonal structure improved the reflection about 2.5 dB in the entire bandwidth.

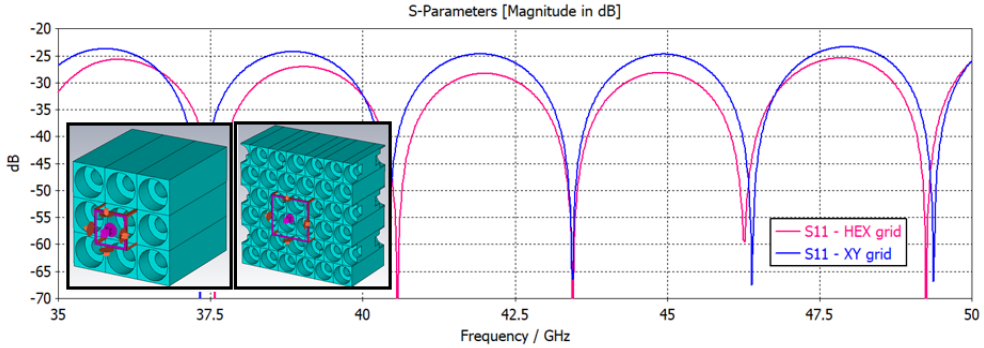

Figure 6 Comparison between the reflection coefficient of the HDPE window with two AR layers in XY grid and Hex configurations

Figure 7 demonstrates the vacuum window plus feed horn and the metal box around the structure acting as dewar walls which are modeled and simulated in CST to analyze the effect of the window on feed horn radiation pattern, and reflection coefficient. Figure 8 depicts the electric field distribution of the feed horn through the vacuum window. As it is shown in Figure 8 and Figure 9, the vacuum window did not cause any reflection back into the feed horn aperture and the reflection coefficient follows the same pattern as with the bare horn.

Downloaded From: https://www.spiedigitallibrary.org/conference-proceedings-of-spie on 14 Dec 2020
Terms of Use: https://www.spiedigitallibrary.org/terms-of-use

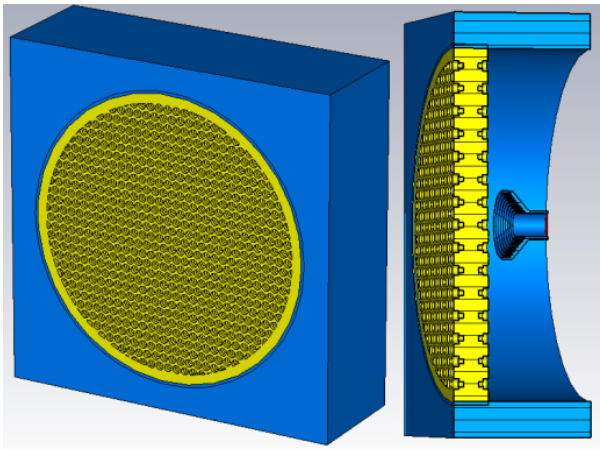

Figure 7 Vacuum window structure

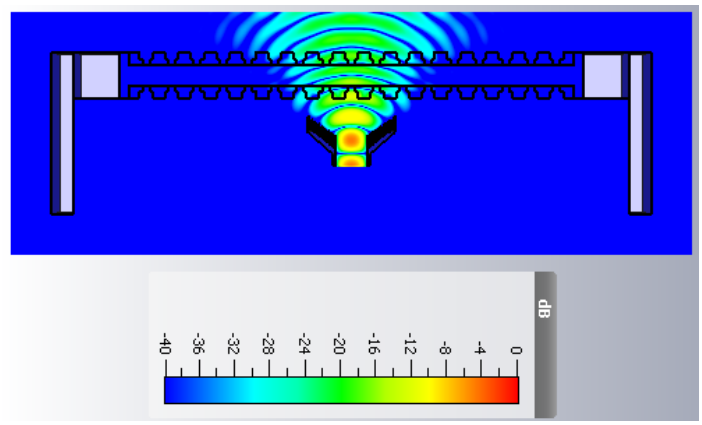

Figure 8 Electric field distribution of the feed horn plus vacuum window

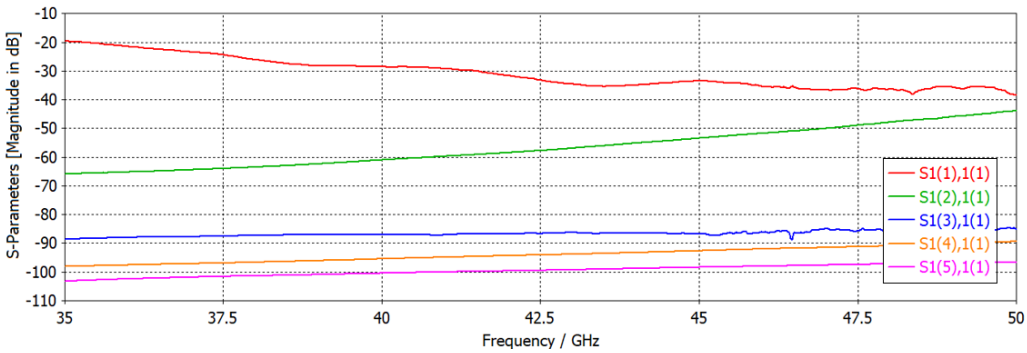

Figure 9 Reflection coefficient of the feed horn plus vacuum window for the first five modes

The CST simulation results for the horn and window were imported into GRASP and used to feed the DVA-2 optics model. The rotational symmetry of the main beam is almost perfect in all cases as is displayed in Figure 10. The first side lobe has some rotational variation depending on the case. The patterns fall off to a very low level beyond the first few side lobes due to the very low edge tapers on both reflectors. The cross polarization levels are very low in all cases. Table 5 summarizes the key performance parameters of an ideal Gaussian beam, the bare feed horn, and feed horn plus the vacuum window (in GRASP) to give us an overall view. The first side lobes (SL1) are nearly constant in all three cases and very close to the DVA-2 design target of -21 dB.

Downloaded From: https://www.spiedigitallibrary.org/conference-proceedings-of-spie on 14 Dec 2020
Terms of Use: https://www.spiedigitallibrary.org/terms-of-use

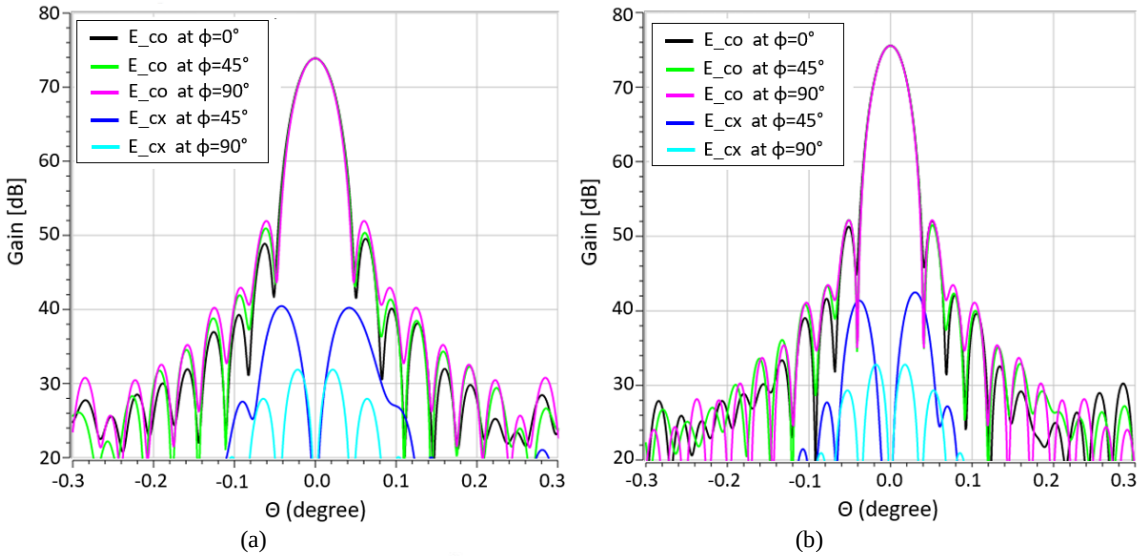

(a) (b)

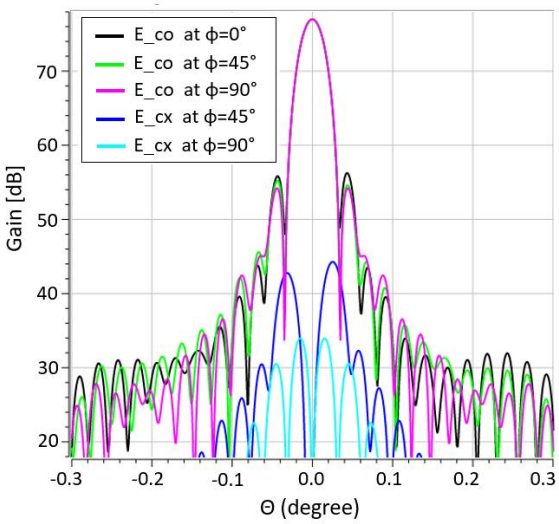

(c)

Figure 10 (a) 35 GHz, (b) 42.5 GHz, (c) 50 GHz beam pattern from GRASP simulation

Table 5 Summary of key performance parameters for all cases (GRASP analysis).

Feed	Freq. (GHz)	Gain (dBi)	AP. eff.	Spill. eff.	Pol. eff.	SL1 [dB]
Ideal Gaussian beam	35	74.05	0.840	0.976	-	-21.9
Bare horn	35	73.88	0.807	0.955	0.998	-22.7
Horn + window	35	73.88	0.807	0.954	0.998	-22.0
Ideal Gaussian beam	42.5	75.70	0.833	0.976	-	-21.8
Bare horn	42.5	75.55	0.804	0.967	0.999	-23.6
Horn + window	42.5	75.56	0.806	0.965	0.999	-23.4
Ideal Gaussian beam	50	77.07	0.825	0.976	-	-21.6
Bare horn	50	77.02	0.815	0.969	0.999	-21.0
Horn + window	50	76.99	0.810	0.972	0.999	-20.7

Downloaded From: https://www.spiedigitallibrary.org/conference-proceedings-of-spie on 14 Dec 2020
Terms of Use: https://www.spiedigitallibrary.org/terms-of-use

5. OMT AND NOISE CALIBRATION MODULE

Figure 11 shows the proposed OMT design for the Q-band receiver. The dual-linear OMT is modeled after the ALMA Band 1 production unit, described as the Version 3 OMT in [4] and [5]. While the design has similarities to the ALMA Band 1 OMT, it also has two integrated 35 dB directional couplers that can be used for noise calibration and the outputs have been phase-matched to preserve the functionality for circular polarization. The noise diode injects the noise through OMT port 4 which is a standard WR-22 waveguide port. The signal passes the first 35 dB directional coupler and then turn 90 degrees and inject the noise into the orthogonal polarization through the second directional coupler. Port 5 is matched and terminated. Therefore, integrating the directional couplers and using one input port for noise injection improves OMT design, avoids using a power divider for the noise injection, so makes the mechanical layout simpler, and decreases the thermal load on the 16 K stage. The noise diode is located in the 300K stage to shield the circuit from signals external to the cryostat.

As it is shown in

Figure 12, simulated return loss is better than 25 dB and the insertion loss is better than 0.28 dB from 35-50GHz. The ports are defined as 1: input from feed horn circular 6.7 mm waveguide, ports 2 and 3: linear X and Y output WR-22, port 4: coupled noise injection input WR-22, and port5 would be terminated by a custom designed piece of Eccosorb MF-117 which acts as an attenuator to terminate the waveguide port with a match better than 35 dB. It is a rigid magnetically loaded epoxy stock, which can be easily machined for use as absorbers, attenuators, and terminations.

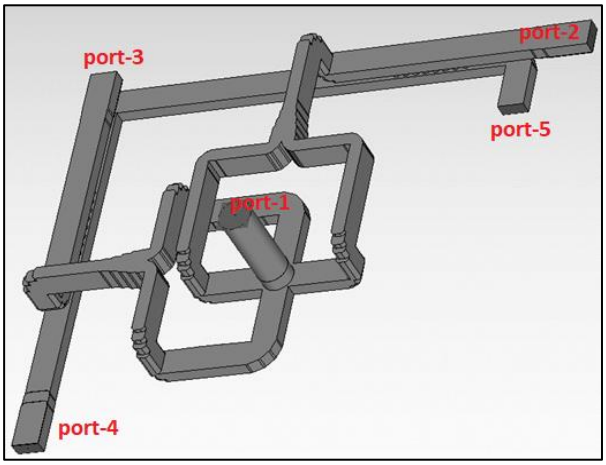

Figure 11 Proposed Q-band OMT including noise couplers for calibration. Outputs have been phase-matched in case circular polarization is needed.

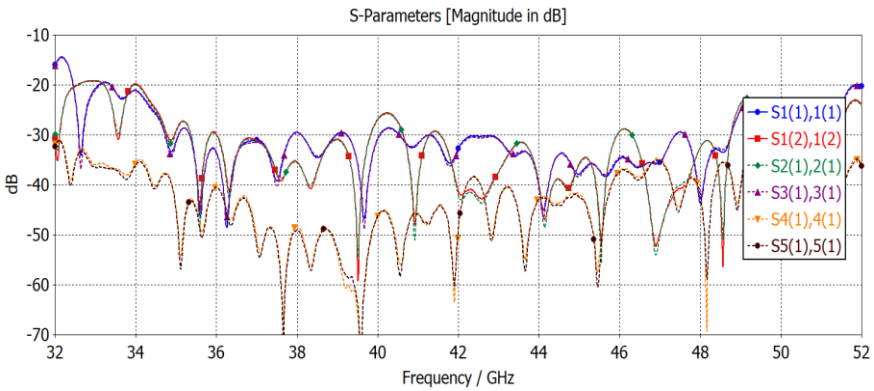

(a)

Downloaded From: https://www.spiedigitallibrary.org/conference-proceedings-of-spie on 14 Dec 2020
Terms of Use: https://www.spiedigitallibrary.org/terms-of-use

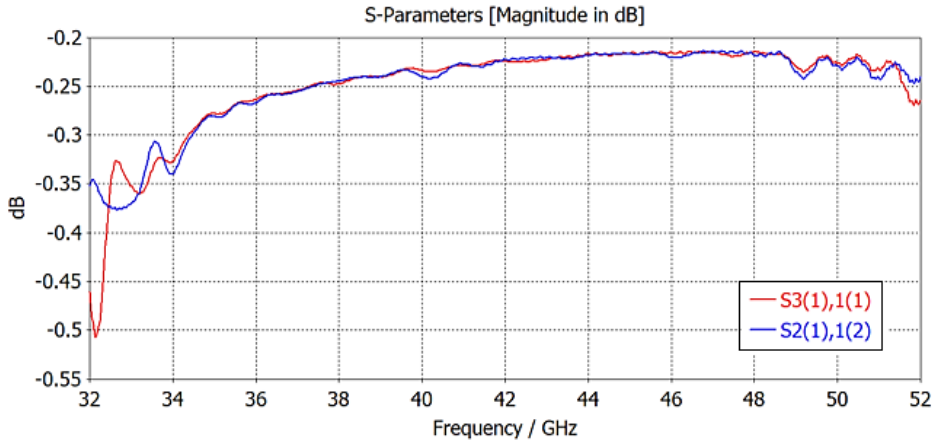

(b)

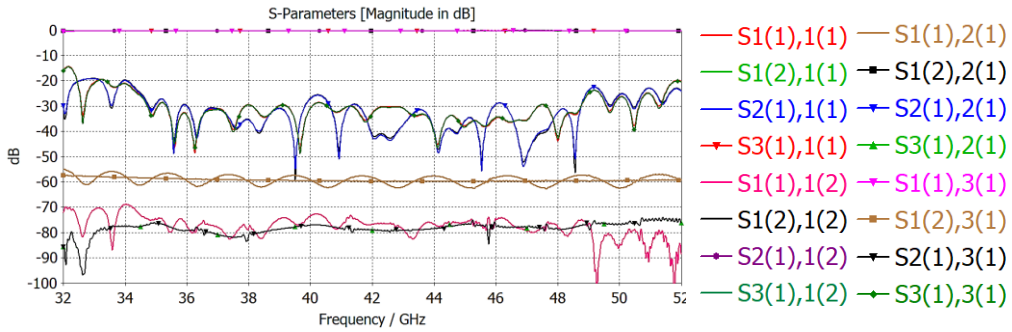

(c)

Figure 12 Performance of the optimized OMT between 32 to 52 GHz (a) input match and cross-pol, (b) insertion loss, (c) the scattering parameters of the OMT

6. LOW NOISE AMPLIFIER

6.1 Cryogenic LNA

The specifications of the proposed cryogenic low noise amplifier with waveguide input and output are presented in Table 6. The proposed design is an mHEMT MMIC LNA design with WR-22 waveguide input and output ports. Q-band LNA waveguide chassis machining work, probe testing, and qualification are completed and 7 chassis are ready for sending out for gold plating. Figure 13 shows the LNA chassis.

Table 6 Low noise amplifier specifications

Frequency	35 – 50 GHz
Gain, S21	≥ 30 dB
Input match, S11	≤ -10 dB
Output match, S22	≤ -10 dB
Isolation	50 dB
Noise temperature	≤ 12 K
Gain flatness	± 1.5 dB

Downloaded From: https://www.spiedigitallibrary.org/conference-proceedings-of-spie on 14 Dec 2020
Terms of Use: https://www.spiedigitallibrary.org/terms-of-use

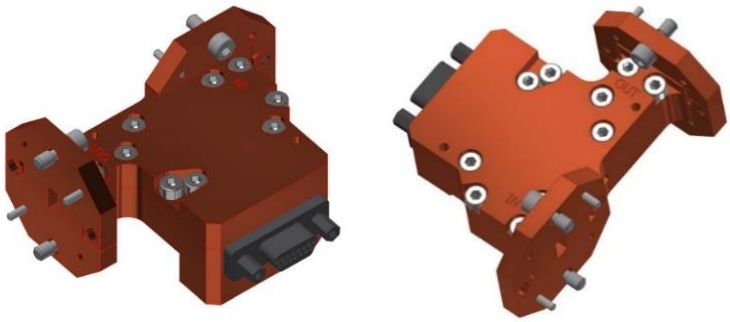

Figure 13 Q-band low noise amplifier chassis with WR-22 input and output ports.

6.2 Post amplification

The specifications of the required LNA are presents in Table 7. A room temperature 4-stage LNA has been designed and fabricated using WIN Foundry 0.15-μm GaAs process. This process offers pHEMT devices with a transit frequency (f_T) of 95 GHz, two layers of metallization, metal-insulator-metal (MIM) capacitors, and backside via holes. The schematic design of the amplifier is shown in Figure 14. The chip is biased at 2.5 V drain voltage and -0.6 V gate voltage with on-chip RF decoupling capacitors and low pass filters for each individual bias line. The effect of input/output and bias wire bonds, 30 mil and 60 mil long, respectively, is taken into account, and the amplifier is optimized for maximum gain and low-noise performance. The fabricated chip, shown in Figure 15, is packaged with a custom designed gold plated chassis with coaxial ports. Figure 16 shows the measured results of the packaged amplifier with the coaxial interface.

Table 7 Post amplifier specifications

Frequency	35-50 GHz
Gain, S21	25 dB
Input match, S11	≤ -10 dB
Output match, S22	≤ -10 dB
Noise figure	≤ 4.5 dB
Noise temperature	≤ 527.33 K

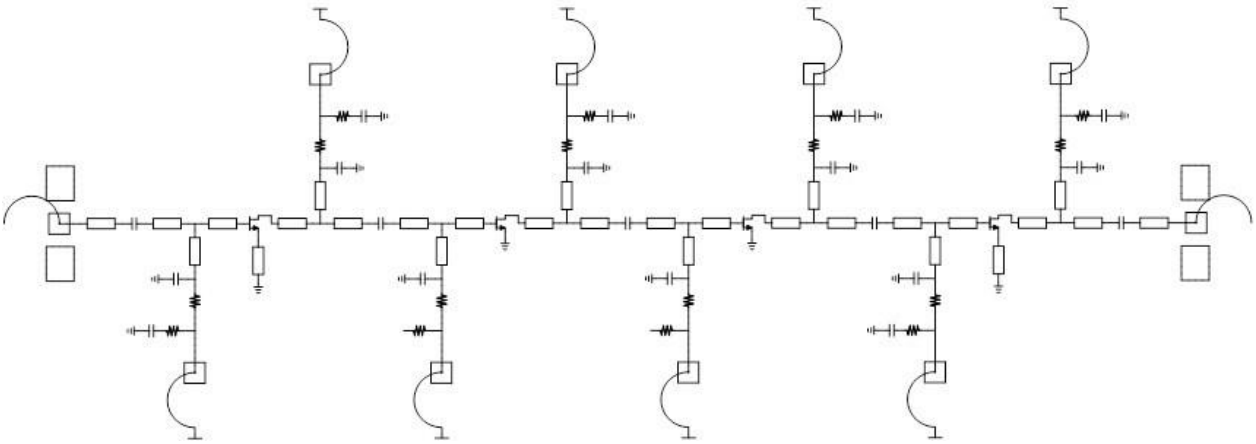

Figure 14 Schematic of the post amplifier (warm LNA)

Downloaded From: https://www.spiedigitallibrary.org/conference-proceedings-of-spie on 14 Dec 2020
Terms of Use: https://www.spiedigitallibrary.org/terms-of-use

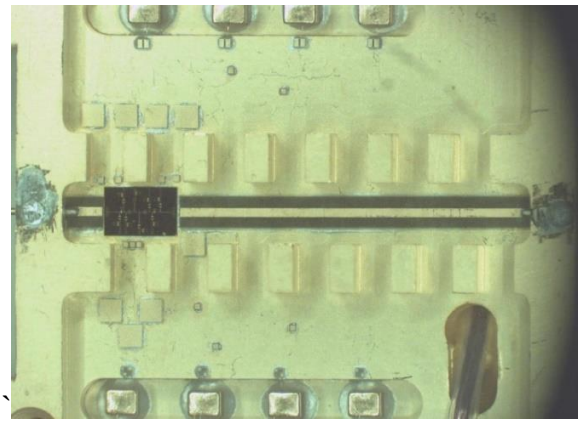

Figure 15 Packaged LNA with gold plated chassis

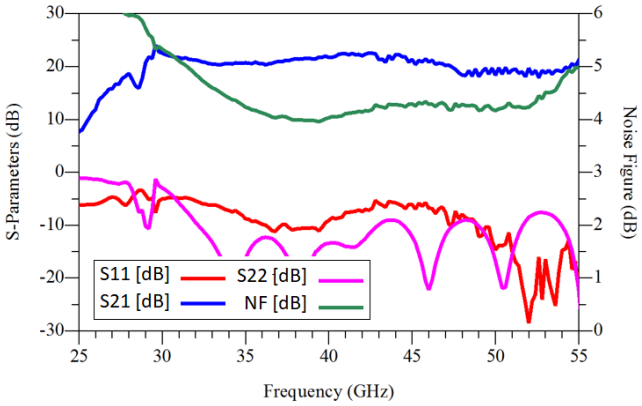

Figure 16 Measurement results of packaged post amplifier

7. DOWN CONVERTER

The RF signal should be down-converted from the RF band of 35-50 GHz to IF band of 8-16 GHz. A proposed mixer is a Gilbert Cell (GC) Double Balanced (DB) mixer with passive baluns at LO and RF port with single ended emitter follower drive followed by a Band Pass Filter at the output. It has 4-6 dB gain and is matched to 50 Ohms at all ports. The structure of the proposed mixer is shown in Figure 17. Table 8 demonstrates the mixer specifications. The mixer is still in the design process.

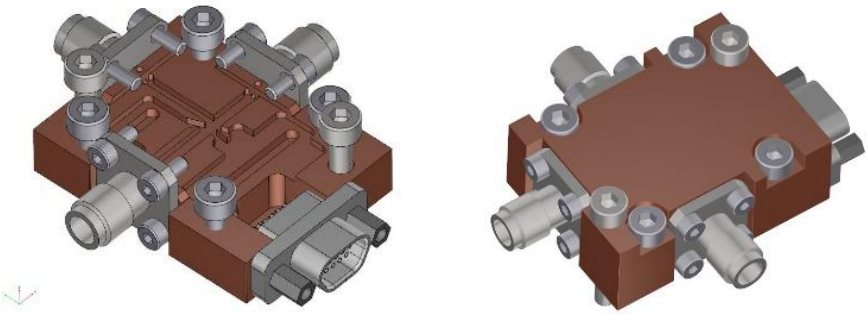

Figure 17 Down-converter / Mixer structure

Table 8 Mixer specifications

Conversion gain (dB)	6
Gain flatness (dB)	2
RF frequency (GHz)	35~50 GHz
LO frequency (GHz)	27 – 34
IF frequency (GHz)	8~16 GHz
RF port return loss (dB)	< -10
IF port return loss (dB)	< -10
LO port return loss (dB)	< -8
LO-RF isolation (dB)	< 35
LO-IF isolation (dB)	17.5
RF-IF isolation (dB)	30
3% input gain compression point (dBm)	-19

Downloaded From: https://www.spiedigitallibrary.org/conference-proceedings-of-spie on 14 Dec 2020
Terms of Use: https://www.spiedigitallibrary.org/terms-of-use

8. CASCADED NOISE ANALYSIS

The cascaded noise analysis of the Q-band receiver consisting of both cryostat and room temperature components are calculated. This analysis includes vacuum window, feed horn, OMT, directional coupler, LNAs, post amplification, filters, and mixer are taken into account. An assumption of 5dB loss is considered for back-end components loss. Table 9 presents the cascaded noise temperature of the Q-band receiver.

Table 9 Cascaded noise analysis of the Q-band receiver,

Column 2: The power gain of the component in dB.
Column 3: Cumulative power gain through all devices.
Column 4: T_{comp} is the calculated noise temperature of the individual component (K),
Column 5: T_{rx} is the cumulative receiver noise temperature from the first optical component cryostat window to back-end cables (K).
Column 6: Actual physical temp of the selected device

Component	**Gain [dB]**	**Cum. Gain [dB]**	**$T_{comp.}$ (K)**	**T_{rx} (K)**	**Phys. Temp (K)**
Vacuum window	-0.014	-0.01	0.96	0.96	300
Feed Horn	-0.018	-0.03	0.06	1.03	16
OMT(integrated coupler)-thru path	-0.3	-0.33	1.14	2.18	16
Calibration coupler-coupled path	0	-0.33	0.09	2.29	300
WG to WG flange	-0.05	-0.38	0.18	2.49	16
LNA	30	29.6	13	16.6	16
WG to coax adaptor	-0.5	29.1	1.95	16.6	16
Stainless steel coax cable	-2	27.1	87.7	16.7	150
Coax cable to noise diode	-1	26.1	77.6	16.9	300
BPFilter (35-50GHz)	-2	24.1	175.4	17.3	300
Post amplification	25	49.1	527.3	19.4	300
Mixer	6	55.1	1716	19.4	300
Back-end cables	-5	50.1	648.6	19.4	300

By using ngVLA sky and spillover noise temperature the system temperature of the proposed Q-band receiver is calculated at four frequencies.

Table 10 System noise temperature of the Q-band receiver

Frequency (GHz)	**T_{rx} (K)**	**T_{spill} (K)**	**T_{sky} (K)**	**η_{feed}**	**T_{sys} (K)**	**T_{sys} / η_{feed}**
35	20.1	4.1	13.5	0.78	36.5	46.8
40	19.5	4.1	17.5	0.79	40.4	51.5
45	20	4.1	30.6	0.79	53.4	67.4
50	20	4.1	70.2	0.81	99.1	121.9

Downloaded From: https://www.spiedigitallibrary.org/conference-proceedings-of-spie on 14 Dec 2020
Terms of Use: https://www.spiedigitallibrary.org/terms-of-use

9. INTEGRATED FRONT-END SYSTEM

The integration of Feed horn, vacuum window, OMT with added 35dB coupler, and metal walls are modeled and simulated in CST Studio full wave electromagnetic simulator. Figure 18 shows a wire frame of the structure. The simulated results show a promising performance and meet the expectations. Figure 19 depicts the co-pol and cross polarization pattern of the integrated model at three frequencies. As it is depicted, the results have a great agreement with the bare horn model presented in section 3. The vacuum window, metal boxes, and the integration of OMT did not cause any extra reflection and did not interfere with the farfield pattern of the receiver.

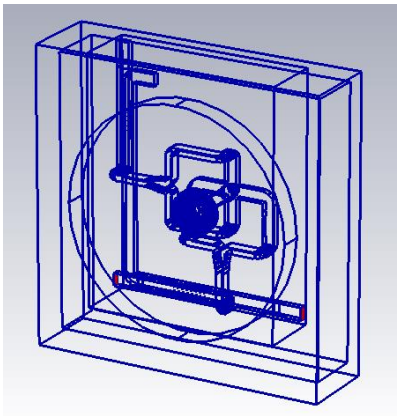

Figure 18 Integration of feed horn, vacuum window, and OMT

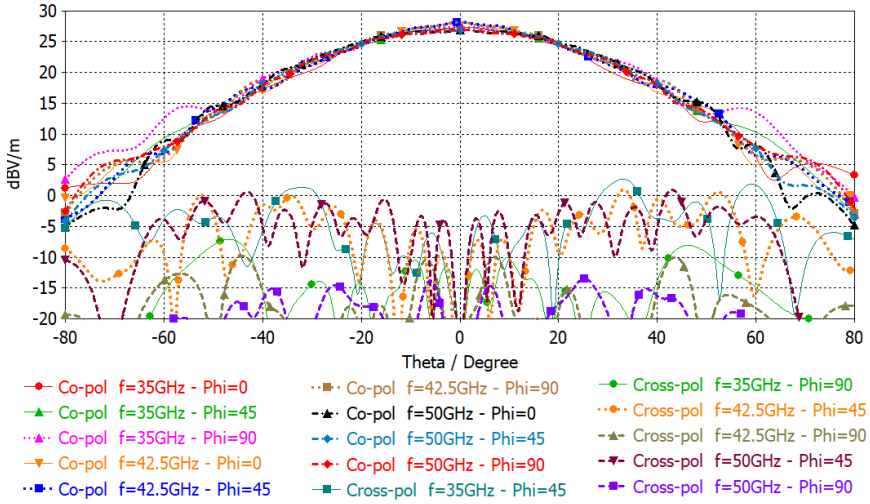

Figure 19 Far-field radiation pattern (co-pol and cross-pol) of the integrated model at 3 frequencies.

10. MECHANICAL DESIGN

The vacuum vessel will be an off-the-shelf configurable, custom ISO-160F T-flange from Kurt J. Lesker. A standard industrial two stage Gifford-McMahon is selected to produce helium closed-cycle refrigeration at two physical temperature 16K and 70K stages. The place of the two cryogenic 16 K and 70 K plates along the axis of the vacuum vessel is determined by dimensions of the cold head and cold finger. Also, the size and location of components located in the 16 K stage including the vacuum window, feed horn, OMT, and LNAs specify the height of the vacuum vessel [1].

All the components located in 16K stage except the feed horn will be surrounded by a 70 K heat shield and a 20 layer aluminized multilayer insulation blanket (RUAG COOLCAT 2 NW). Stainless steel coaxial cables are used to obtain

Downloaded From: https://www.spiedigitallibrary.org/conference-proceedings-of-spie on 14 Dec 2020
Terms of Use: https://www.spiedigitallibrary.org/terms-of-use

thermal insulation between the LNA outputs and the 300 K cryostat output hermetic feedthroughs, and also between the directional coupler input and the noise diode in 300K stage. An external shield to prevent condensation on the window will be installed. This external shield will be a thin layer (tens of microns) of HDPE.

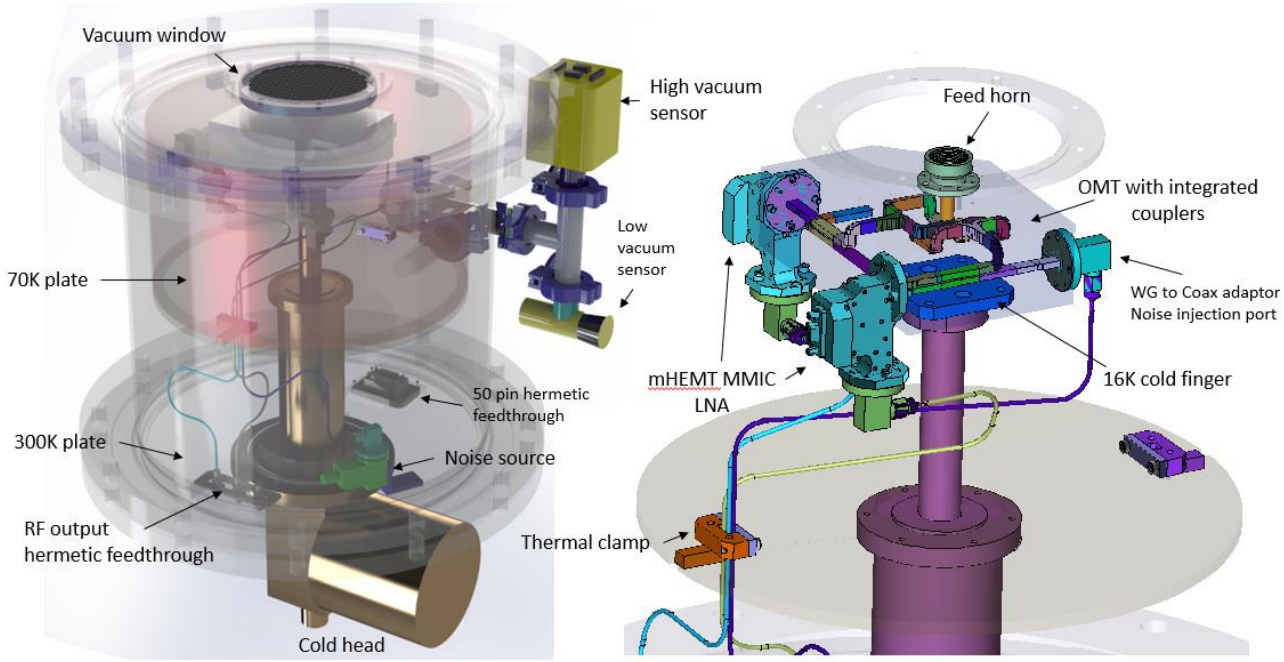

Figure 20 Mechanical layout of the Q-band receiver cryostat

11. INDEXER

The DVA-2 feeds are split up into low and high frequency – low being 0.35-2 GHz and high 2-50GHz.

Because of the potential for minor structural and dish deflection in operation, high frequency feeds require adjustment on 3 axes, dependent on dish elevation. Low only need Z-adjustment. The specification of the design for mounting feeds capable of receiving up to 50 GHz:

- Total positioning accuracy of 1/20 of 6 mm wavelength – 300 microns
- Control system sensing resolution of 1/10 positional accuracy – 30 microns

Figure 21 shows the final structure of the indexer which will be installed on DVA-2 dish, and Figure 22 presents the control system. There will be locations for 4 receivers on the indexer. All will have a z-direction adjustment for focusing and two will have full x-y-z positioning and will be reserved for high frequency receivers. Servomotor linear actuators drive the independent stages of the positioner. The servomotor feedback is adequate for positioning accuracy, provided that the positioning error associated with the indexer structure deflection is low. External encoders are available to improve positioning feedback.

Downloaded From: https://www.spiedigitallibrary.org/conference-proceedings-of-spie on 14 Dec 2020
Terms of Use: https://www.spiedigitallibrary.org/terms-of-use

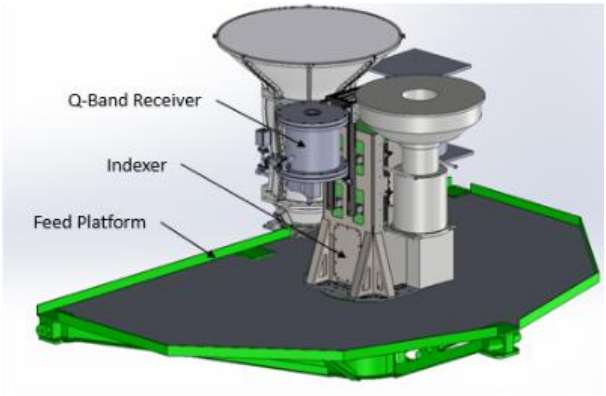

Figure 21 Indexer with full feed compliment

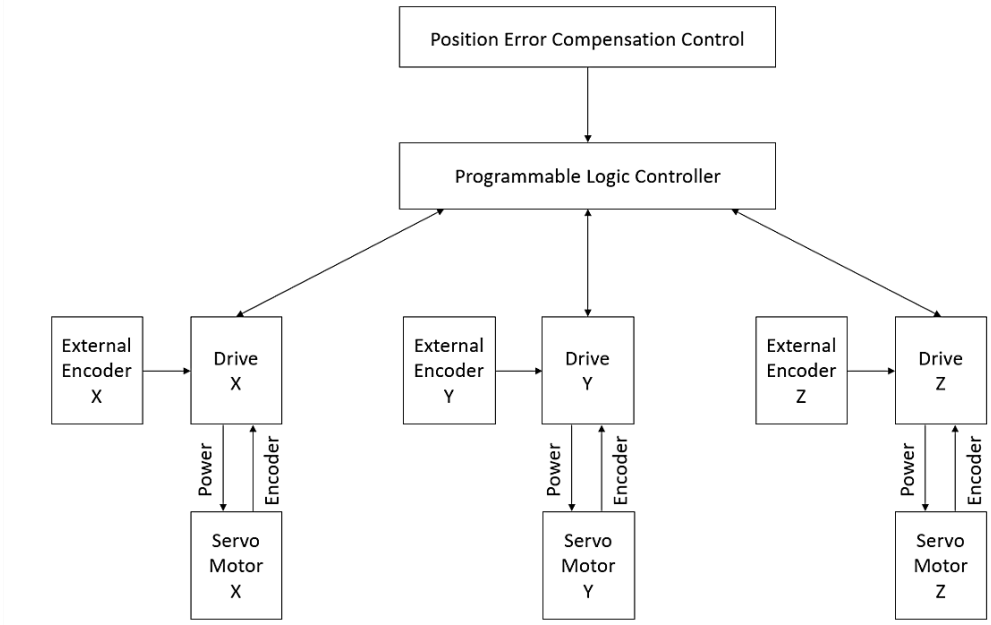

Figure 22 Control system

SUMMARY

A front-end system is presented for a dual-linear polarization cryogenic Q-band (35–50 GHz) receiver intended to demonstrate DVA-2 antenna performance and as a technology demonstrator. The first stage of the cryostat includes a feed horn, a compact noise calibration module (NCM) integrated with an OMT, and two mHEMT MMIC LNAs located in the 16K stage. The proposed cryogenic receiver provides an estimated noise temperature around 19.4 K. The vacuum window and feed horn have an excellent performance, comparable to the ideal Gaussian beam through the bandwidth. The OMT with integrated noise calibration couplers has low loss and compact design with return loss better than 25dB and insertion loss better than 0.28 dB between 35-50GHz.

ACKNOWLEDGEMENTS

The authors would like to acknowledge our former co-op student, Luke Evans for implementing a Post-Processing Template using VBA Macros for efficiency calculations.

Downloaded From: https://www.spiedigitallibrary.org/conference-proceedings-of-spie on 14 Dec 2020
Terms of Use: https://www.spiedigitallibrary.org/terms-of-use

REFERENCES

[1] Locke L., Baker, L.A., Henke, D., Jiang, F., Knee, L., and Reshetov, V., "Q-band single pixel receiver development for the ngVLA and NRC", Proceedings, SPIE Astronomical Telescopes + Instrumentation, Volume 10708, Austin, Texas, United States, 2018.

[2] Islam, M., and Lacy, G., "An improved secondary reflector for DVA-2 radio telescope: a case study on application of structural optimization technique", Proceedings, SPIE Astronomical Telescopes + Instrumentation, Volume 10700, Austin, Texas, United States, 2018.

[3] Baker, L., and Imbriale, W.A., "Optical Design of DVA-1, A Prototype Antenna for the SKA Mid-Band Array", Proceedings, 16th International Symposium on Antenna Technology and Applied Electromagnetics (ANTEM), Victoria, BC, Canada, 2014.

[4] Henke, D., and Claude, S., "Minimizing RF Performance Spikes in a Cryogenic Orthomode Transducer (OMT)", IEEE Trans. Microwave Theory Tech, vol. 62(4), pp. 840-850, 2014.

[5] Hwang, Y.-J., Chiong, Huang, T., "ALMA Band 1 Cartridge Critical Design Review Design Report," Doc: FEND-40.02.01.00-0089-A-DSN, Nov., 2015.

Downloaded From: https://www.spiedigitallibrary.org/conference-proceedings-of-spie on 14 Dec 2020
Terms of Use: https://www.spiedigitallibrary.org/terms-of-use